

Article

## Improving Estimates of Grassland Fractional Vegetation Cover Based on a Pixel Dichotomy Model: A Case Study in Inner Mongolia, China

Fei Li <sup>1</sup>, Wei Chen <sup>2</sup>, Yuan Zeng <sup>1</sup>, Qianjun Zhao <sup>1</sup> and Bingfang Wu <sup>1,\*</sup>

<sup>1</sup> Key Laboratory of Digital Earth Science, Institute of Remote Sensing and Digital Earth, Chinese Academy of Sciences, Olympic Village Science Park, W. Beichen Road, Beijing 100101, China; E-Mails: lfgis@163.com (F.L.); zengyuan@radi.ac.cn (Y.Z.); zhaoqj@radi.ac.cn (Q.Z.)

<sup>2</sup> School of Geosciences and Info-Physics, Central South University, Changsha 410083, China; E-Mail: lajiao.1225@163.com

\* Author to whom correspondence should be addressed; E-Mail: wubf@radi.ac.cn; Tel.: +86-10-6485-5689; Fax: +86-10-6485-8721.

Received: 27 February 2014; in revised form: 9 May 2014 / Accepted: 14 May 2014 /

Published: 26 May 2014

---

**Abstract:** Linear spectral mixture analysis (SMA) is commonly used to infer fractional vegetation cover (FVC), especially for pixel dichotomy models. However, several sources of uncertainty including normalized difference vegetation index (NDVI) saturation and selection of endmembers inhibit the effectiveness of SMA for the estimation of FVC. In this study, Moderate-resolution Imaging Spectroradiometer (MODIS) and Landsat 8/Operational Land Imager (OLI) remote sensing data for the early growing season and *in situ* measurement of spectral reflectance are used to determine the value of endmembers including  $VI_{soil}$  and  $VI_{veg}$ , with equally weighted RVI and NDVI measures used in combination to minimize the inherent biases in pure NDVI-based FVC. Their ability to improve estimates of grassland FVC is analyzed at different resolutions. These are shown to improve FVC estimates over NDVI-based SMA models using fixed values for the endmembers. Grassland FVC changes for Inner Mongolia, China from 2000 to 2013 are then monitored using the MODIS data. The results show that changes in most grassland areas are not significant, but in parts of Hulunbeier, south Tongliao, middle Xilin Gol and Erdos, grassland FVC has increased significantly.

**Keywords:** grassland; fractional vegetation cover; pixel dichotomy model; Inner Mongolia; MODIS; Landsat 8

---

## 1. Introduction

The ratio of the vertical projected area of vegetation to the total ground area, termed fractional vegetation cover (FVC), is a commonly used indicator for evaluating and monitoring vegetation degradation and desertification [1]. Several methods for retrieval of FVC using remote sensing have been developed including spectral mixture analysis (SMA) [2–4], artificial neural networks [5–7], fuzzy classifiers [8], maximum likelihood classifiers [9], regression trees [10–12], and simple regression based on the Normalized Difference Vegetation Index (NDVI) [13]. In particular, SMA has often been used to estimate FVC from multi-spectral remote sensing data [2,14–18].

SMA utilizes pure spectral components, called endmembers, to simulate the proportions in a pixel, assuming that a pixel value in multi- or hyper- spectral imagery can be decomposed into a proportional representation of the materials contributing to the overall pixel signal [19,20]. SMA with fixed or variable endmembers has been used for the estimation of FVC in various environments including arid/semi-arid regions [21–24] and at scales from regional to global [25–28]. For grassland, linear SMA models with two endmembers (vegetation and non-vegetation) or three endmembers (live grass, senesced grass and soil) are effective in estimating endmember fractions due to their simplicity and interpretability [2–4,13,29]. In particular, two-endmember models based on NDVI simplify the endmember selection process and substantially improve computational efficiency [30].

The two-endmember model is assumed to have a unique spectral signature for each endmember, with the spectral variability within an endmember minimal and negligible [30]. However, it is always challenging to select representative endmembers, which are critical for the success of a mixture model. Several approaches have been used for the retrieval of image endmembers including the use of two-dimensional feature space plots [31] and the identification of pure pixels with reference to field data or higher-resolution remote sensing data [32]. In most cases, these approaches assume a constant endmember signature (e.g., for bare soil or for full vegetation cover) even with large changes in the land surface. To our knowledge, the impact on estimation accuracy of using a constant endmember has not been seriously considered.

Another challenge for SMA is the selection of the models' parameters. Numerous studies use a vegetation index (VI) as a signal or signature to maximize the differences among the endmembers. For example, NDVI based SMA has been used to estimate FVC in a large number of landscapes with various remote sensing data sources [26,33–35]. However, NDVI has been criticized because FVC tends to be overestimated as it approaches certain proportions [36], especially in moderately vegetated areas [1,37].

To improve the ability of SMA models to estimate FVC, this study: (1) evaluates the influence of different VIs, including NDVI and RVI, on FVC estimation at different resolutions; (2) suggests the use of a weighted combination of NDVI and RVI in SMA models to cancel out the biases of NDVI or RVI when used alone; and (3) proposes a simplified endmember selection process for SMA models

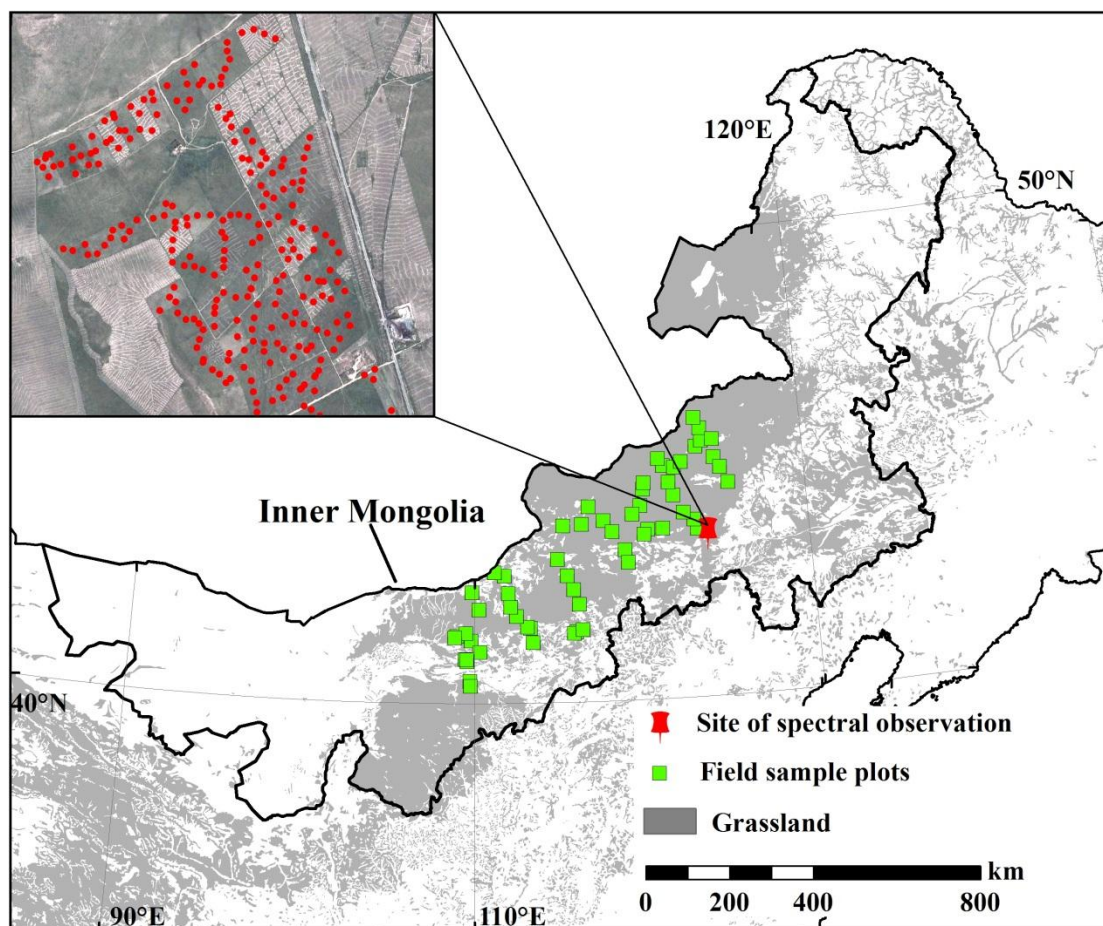
through the use of remote sensing data in the early growing season and *in situ* measurement of spectral reflectance.

## 2. Data and Methods

### 2.1. Study Area

The study was conducted in the Inner Mongolia grasslands of northern China (Figure 1), with grassland distribution determined from vegetation maps (at a scale of 1:1 million) compiled by a committee of the Chinese Academy of Sciences in 2001. The area has a temperate continent monsoon climate with mean annual temperatures decreasing from about 9 °C in the southwest to −5 °C in the northeast. Annual rainfall varies from 150 to 500 mm, 80% of which occurs in the May to October growing season. In contrast to temperature, annual rainfall increases from the southwest to the northeast. Topographically, the area is dominated by plateaus with the Ordos, Xilingole and Hulun Buir plateaus arrayed from the southwest to the northeast. Grassland covers about 70% of the area but most is sparsely vegetated [38,39], with desert steppe, typical steppe and meadow steppe being the primary types [40].

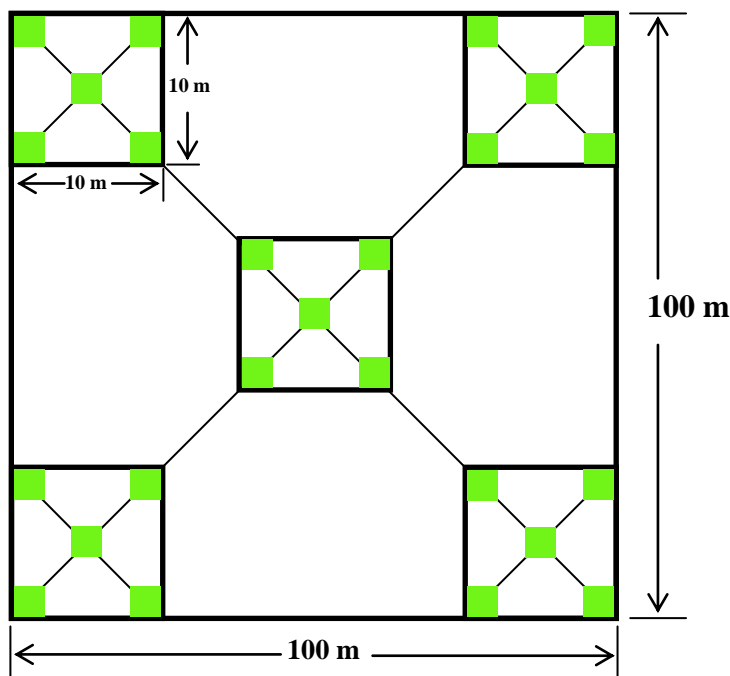
**Figure 1.** Site of spectral measurement and distribution of sample plots.



## 2.2. Field Data

Field data was collected in central Inner Mongolia from 20 July to 10 August 2013. A Trimble GPS was used to obtain the coordinates for the sample plots (see Figure 1) and fisheye camera photographs were acquired for FVC estimation. Plot design is shown in Figure 2. Fifty sample plots each  $100 \times 100$  m were aimed at evaluating results from the Moderate-resolution Imaging Spectroradiometer (MODIS) data, which has a resolution of 250 m, and 250 sample plots each  $10 \times 10$  m were aimed at evaluating results from Landsat 8 data, which has a resolution of 30 m. In addition, on 2–6 August 2012, at the Inner Mongolia Grassland Research Station (IMGERS) located at  $116^{\circ}42'E$ ,  $43^{\circ}38'N$ , high resolution portable field spectroradiometers were used to collect spectral reflectance (which ranges from 350 to 2500 nm, with a  $25^{\circ}$  field of view) over the vegetation canopy, together with fisheye camera photographs. The aim here was to obtain the signatures of endmembers (bare soil and full vegetation cover) and enable evaluation of results at the canopy scale. Quadrats with a diameter of approximately 0.5 m (shown by the red symbols in the inset image in Figure 1) were used.

**Figure 2.** Design of sample plots. The sample plot is  $100 \times 100$  m, which is made up of five smaller sample plots each  $10 \times 10$  m distributed along the diagonal. Similarly, each  $10 \times 10$  m plot is made up of five sites with the same distribution as the  $10 \times 10$  m plots. The fisheye camera photographs are then taken around each site.



The “true” value of FVC for quadrats is important for evaluating SMA models. It has been assessed by several methods including manual visual interpretation [37] and automatic and semi-automatic classification [41] of digital photographs. Alternatively, the FVC of quadrats can be measured using the formula:

$$f_c = \frac{\text{Number of pixels with } VI_{RG} \text{ greater than } 0}{\text{Total number of pixels}} \quad (1)$$

$$VI_{GR} = \frac{DN_G - DN_R}{DN_G + DN_R} \quad (2)$$

where  $f_c$  is the measured FVC used for evaluating the estimation accuracy of the models,  $VI_{GR}$  is the normalized green vegetation index used to classify the fisheye photographs, and  $DN_G$  and  $DN_R$  are the green and red channels of the fisheye photographs.

### 2.3. Remote Sensing Data

Remote sensing data from MODIS and Landsat 8 were used in this study. MODIS is an optical sensor onboard the Terra and Aqua satellites, launched in December 1999 and May 2002, respectively, as part of the NASA Earth Observing System. MODIS scans twice daily, acquiring data in 36 spectral bands. Bands 1–2, 3–7 and 8–36 have spatial resolutions of 250 m, 500 m and 1000 m, respectively. The MODIS Land Science Team also provides a suite of standard MODIS data products to users, including the Surface Reflectance 8-Day product (MOD09Q1) with red band (620–670 nm) and near-infrared band (841–875 nm) at a spatial resolution of 250 m. There are 46 eight-day composites in a year, starting at 1 January each year. The MOD09Q1 data products on the accrued day of 97 (7 April 2013) and 217 (5 August 2013) were downloaded from the website [42].

Landsat 8, developed jointly by the National Aeronautics and Space Administration (NASA) and the United States Geological Survey (USGS), is a successor satellite to Landsat 7 aimed at extending the almost 40-year Landsat data archive [43]. It was launched on 11 February 2013 and has two sensors: the Operational Land Imager (OLI) and the Thermal Infrared Sensor (TIRS). OLI collects image data for nine shortwave spectral bands over a 185 km swath with a 30 m spatial resolution for all bands except the 15 m panchromatic band [43]. Level 1 data products containing well calibrated and co-registered OLI and TIRS data are available for free download from the website [44]. Based on the needs of this study, OLI data products between 1 April and 1 May 2013 (the earliest availability of Landsat 8 data products) and between 20 July and 15 August 2013 (the time of field data collection) were downloaded.

Atmospheric radiometric correction of the OLI imagery was conducted using the FLAASH module in the ENVI 5.0 software package (with sp5, hotfix envi50sp3\_r4.exe, issued 30 July 2013). This module, which is based on the MODTRAN4 radiometric transmission model, is considered to be one of the most accurate atmospheric radiometric correction methods for the preprocessing of remote sensing data [1].

Finally, using the latitude and longitude coordinates of the center of the field survey sample plots, spectral reflectance values were extracted from the MOD09Q1 and Landsat 8 data based on 72 m and 7.2 m radii, respectively, to calculate VI.

### 2.4. Pixel Dichotomy Model

The pixel dichotomy model, originally proposed by Adams, Smith and Johnson [3], assumes that signal response (reflectance) for a pixel in a remote sensing image consists of a mix of signals from multiple components which are decomposable based on the areal proportion of the components. In the case of grassland, vegetation and non-vegetation (that is, soil) are the main components. Therefore,

signal  $S$  as received by the remote sensor, can be expressed as a mixture of vegetated signal  $S_v$  and soil signal  $S_s$ , Equation (3) according to the vegetated areal proportion  $f_c$  in a pixel Equations (4) and (5).

$$S = S_v + S_s \quad (3)$$

$$S_v = f_c \times S_{veg} \quad (4)$$

$$S_s = (1 - f_c) \times S_{soil} \quad (5)$$

$S_{veg}$  and  $S_{soil}$  are the signals of a pure pixel, corresponding to full vegetation cover and non-vegetation cover (bare soil), respectively. These are termed endmembers.

Accordingly, FVC can be estimated by the following formula:

$$f_c = \frac{S - S_{soil}}{S_{veg} - S_{soil}} \quad (6)$$

To further improve the ability of this model to estimate FVC, signal  $S$  can be replaced by a  $VI$  to maximize the differences between vegetated and non-vegetated areas and minimize atmospheric impact [35].  $f_c$  can then be expressed as:

$$f_c = \frac{VI - VI_{soil}}{VI_{veg} - VI_{soil}} \quad (7)$$

where  $VI_{soil}$  and  $VI_{veg}$  are  $VI$  for pure pixels, corresponding to bare soil and full vegetation cover, respectively.

Many  $VI$ s can be used to replace  $S$  in Equation (7), such as the commonly used NDVI Equation (8), or the seldom used RVI Equation (9):

$$NDVI = \frac{\rho_{nir} - \rho_{red}}{\rho_{nir} + \rho_{red}} \quad (8)$$

$$RVI = \frac{\rho_{nir}}{\rho_{red}}, \text{ or } \frac{1 + NDVI}{1 - NDVI} \quad (9)$$

where  $\rho_{red}$  and  $\rho_{nir}$  are reflectance for the red and near infrared bands, respectively.

### 3. Results

#### 3.1. Evaluating the Pixel Dichotomy Model at the Quadrat Scale

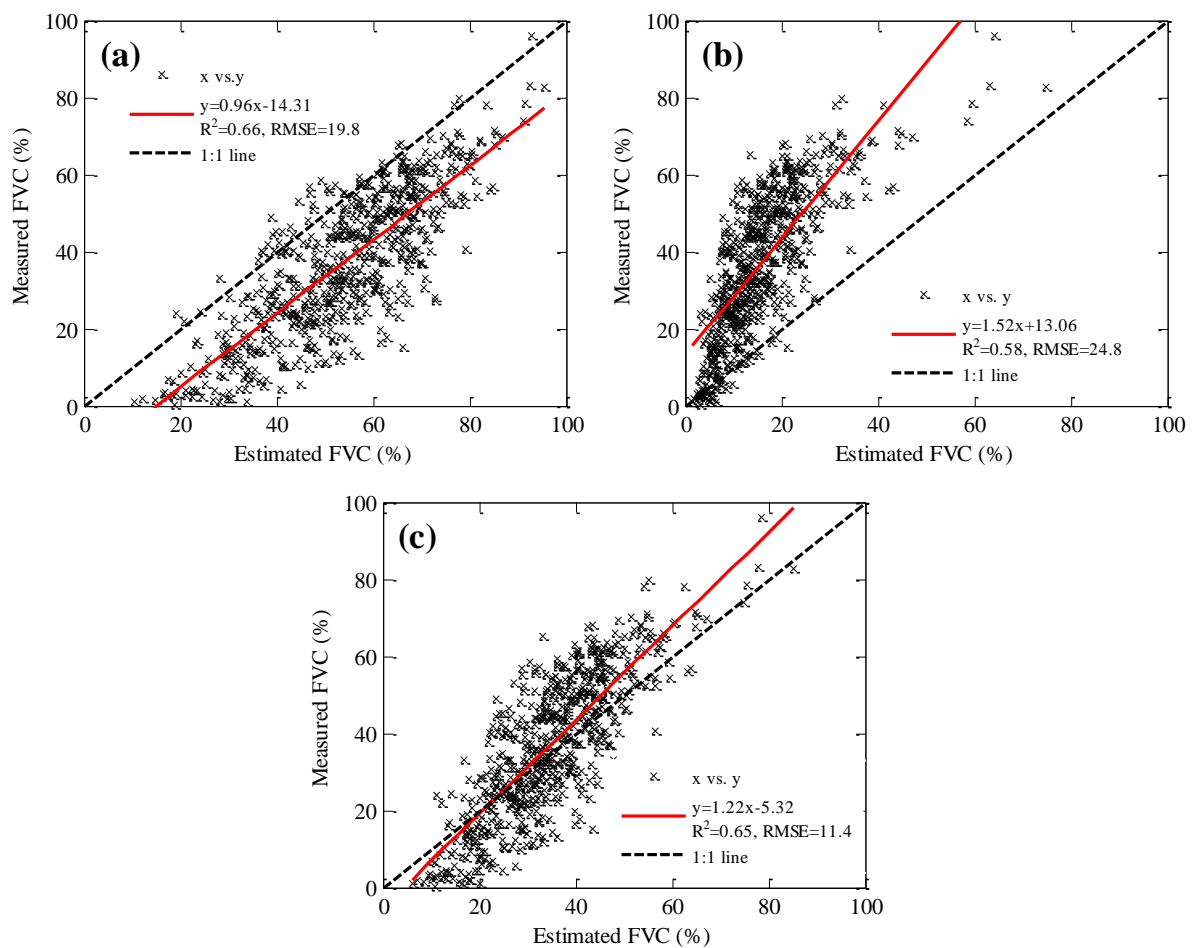
The quadrat grassland FVC at the site of each *in situ* spectral measurement (the red points in the Figure 1) was estimated using Equation (7), with both NDVI and RVI as the parameters of the pixel dichotomy models.  $VI_{soil}$  and  $VI_{veg}$  pure endmembers were derived from *in situ* spectrum measurements (Table 1). NDVI and RVI were calculated from canopy spectrum, with the red and near infrared band resampled based on 250 m MODIS data bands. When NDVI was used, FVC was overestimated due to the saturation of NDVI for high FVC (Figure 3a). When RVI was used, FVC was underestimated as shown in Figure 3b. This is because RVI is less sensitive to low FVC than to high FVC. Figure 3c shows that estimation accuracy can be improved using Equation (10). This combines the two indices and produces a markedly lower RMSE compared with Figure 3a,b.

$$f_c = 0.5 \times \frac{NDVI - NDVI_{soil}}{NDVI_{veg} - NDVI_{soil}} + 0.5 \times \frac{RVI - RVI_{soil}}{RVI_{veg} - RVI_{soil}} \tag{10}$$

**Table 1.** VI values for endmembers derived from *in situ* measurement of canopy spectrum.

	VIs	NDVI	RVI
Endmembers			
$VI_{soil}$		0.203	1.508
$VI_{veg}$		0.891	17.347

**Figure 3.** Accuracy comparison for estimation of grassland FVC at the quadrat scale. (a) using NDVI and (b) using RVI and (c) averaging the results from (a) and (b).



### 3.2. Evaluating Pixel Dichotomy Model at the Pixel Scale

It is a greater challenge to identify the “pure” vegetation and soil pixels from an image than to determine endmember information at the quadrat scale [35]. Generally,  $VI_{veg}$  and  $VI_{soil}$  values are determined by retrieving the maximum and minimum VI values from contiguous areas of high-density vegetation and bare soil within the image [25]. However, due to changes in roughness, soil type and color, this is not necessarily ideal [35]. Given the growing regime for grassland vegetation, data on the land surface during the early growing season represents a soil background composed of bare soil and senesced grass. This is usually interspersed in grassland areas even during the height of the growing

season. Therefore, remote sensing data from the early growing season, specifically on accrued day 97 (7 April 2013) in a year was collected to calculate  $VI_{soil}$  values. Equation (10) can then be expressed as:

$$f_c = 0.5 \times \frac{NDVI - NDVI_{t0}}{NDVI_{veg} - NDVI_{t0}} + 0.5 \times \frac{RVI - RVI_{t0}}{RVI_{veg} - RVI_{t0}} \tag{11}$$

where  $t0$  designates remote sensing data from the early growing season and  $veg$  designates the value for full vegetation cover (FVC = 100%). RVI is calculated from Equation (9).

Unfortunately, obtaining  $VI_{veg}$  pure pixel endmember information solely from moderate and low resolution remote sensing imagery (such as Landsat TM and MODIS) is almost impossible. *In situ* measurements and/or high-resolution remote sensing data are required. Figure 4 shows the spectral reflectance values of bare soil from three sources: *in situ* spectrum measurement, MODIS, and Landsat.  $NDVI_{soil}$  from *in situ* measurement is 0.203, from MODIS data it is 0.118, and from Landsat 8 data it is 0.117. Clearly, there is a substantial spectral signal gap between the different sensors in spite of the same underlying surface. The reasons for this are complex and diverse, including the impacts of atmospheric conditions and scale effects. In order to derive  $VI_{veg}$  for the MODIS and Landsat 8 remote sensing images from the *in situ* measurement of spectral reflectance values for “pure” vegetation and soil (shown in Figure 4), the spectral signal gap for different sensors ( $\Delta NDVI$  in Equation (12)) is assumed to be stable and constant. The pure pixel endmember value for vegetation for the MODIS and Landsat 8 images (denoted as  $NDVI_{pixel\_veg}$ ) is then determined by using  $NDVI_{veg}$  from the *in situ* spectral data measurements and  $\Delta NDVI$  Equation (13). A corresponding set of equations is constructed for RVI. The results are shown in Tables 2 and 3.

$$\Delta NDVI = NDVI_{soil} - NDVI_{pixel\_soil} \tag{12}$$

$$NDVI_{pixel\_veg} = NDVI_{veg} - \Delta NDVI \tag{13}$$

**Figure 4.** Spectral reflectance of bare soil and vegetation for different data sources. The bare soil spectrum and full vegetation spectrum are from *in situ* measurements.

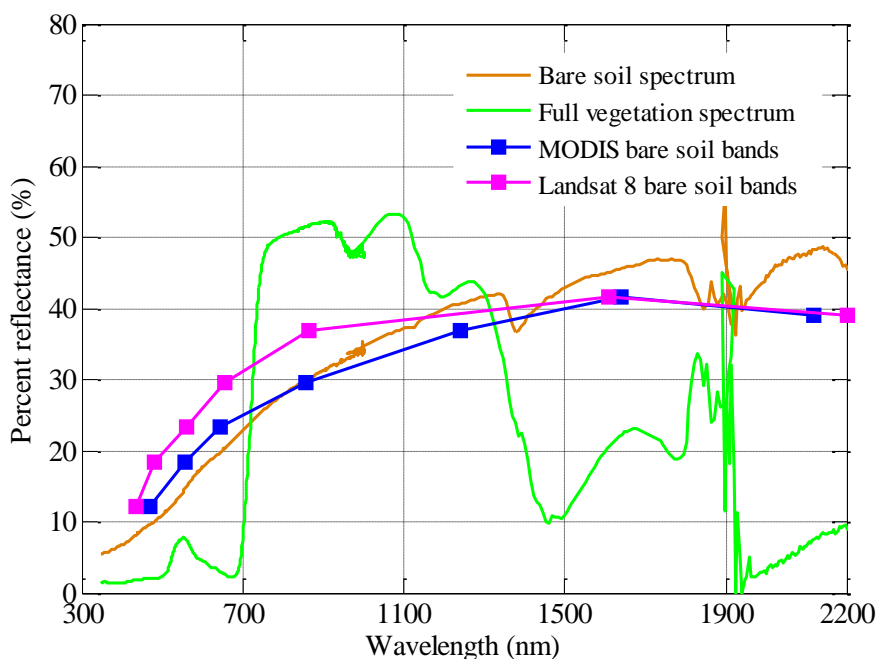


**Table 2.** VI values of endmembers for MODIS.

Endmembers \ VIs	NDVI	RVI
$VI_{soil}$	0.118	1.268
$VI_{veg}$	0.806	9.309

**Table 3.** VI values of endmembers for Landsat 8.

Endmembers \ VIs	NDVI	RVI
$VI_{soil}$	0.119	1.27
$VI_{veg}$	0.807	9.363

Figures 5 and 6 provide accuracy comparisons for estimating grassland FVC for the 250 m and 30 m pixels. Estimation accuracy is improved by using remote sensing data from the early growing season (Figures 5b and 6b) rather than a fixed value for  $NDVI_{soil}$  (Figures 5a and 6a). More importantly, it simplifies the selection of the endmember for  $NDVI_{soil}$ . However, the problems of FVC overestimation using NDVI and underestimation using RVI still exist (Figure 5c vs. 5b and Figure 6c vs. 6b). Figures 5d and 6d show that using Equation (11), which averages NDVI and RVI, can produce relatively good results for estimating grassland FVC with minimal RMSE.

**Figure 5.** Accuracy comparisons for estimating grassland FVC for 250 m pixels. (a) uses NDVI as the parameters of Equation (7), where  $NDVI_{soil}$  is 0.118, and  $NDVI_{veg}$  is 0.806 (Table 2); (b) and (c) use NDVI and RVI, respectively, as the parameters of Equation (11), where  $NDVI_{veg}$  is also equal to 0.806, but  $NDVI_{soil}$  and  $RVI_{soil}$  were calculated using remote sensing data from the early growing season (accrued day 97 for 2013) for soil background measurement; and (d) averages the results from (b) and (c). NDVI and RVI were extracted from MODIS data based on the coordinates of sample plots.

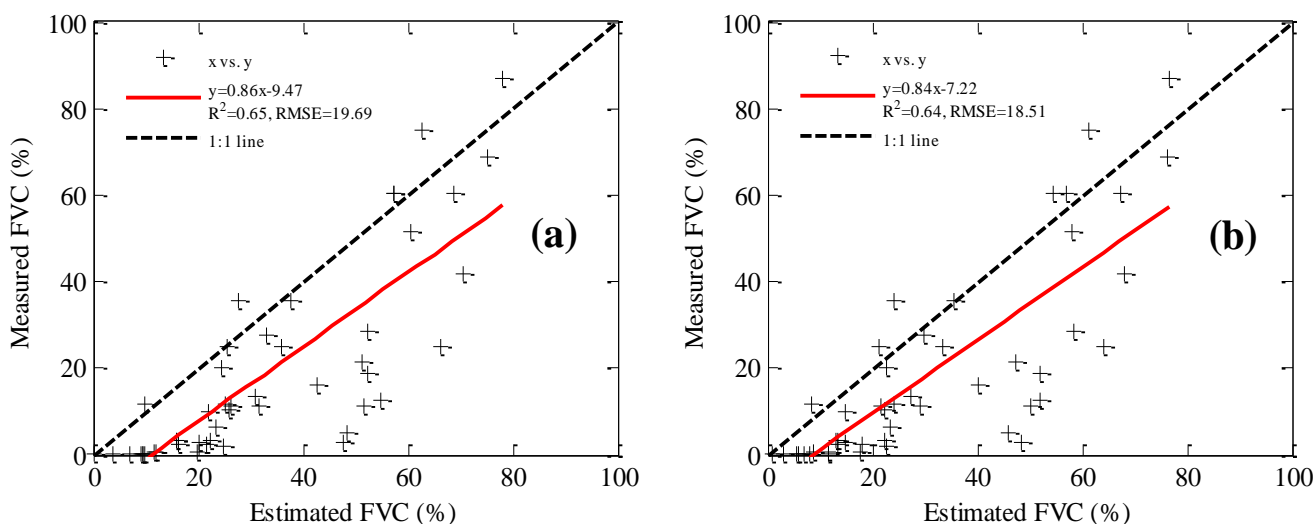
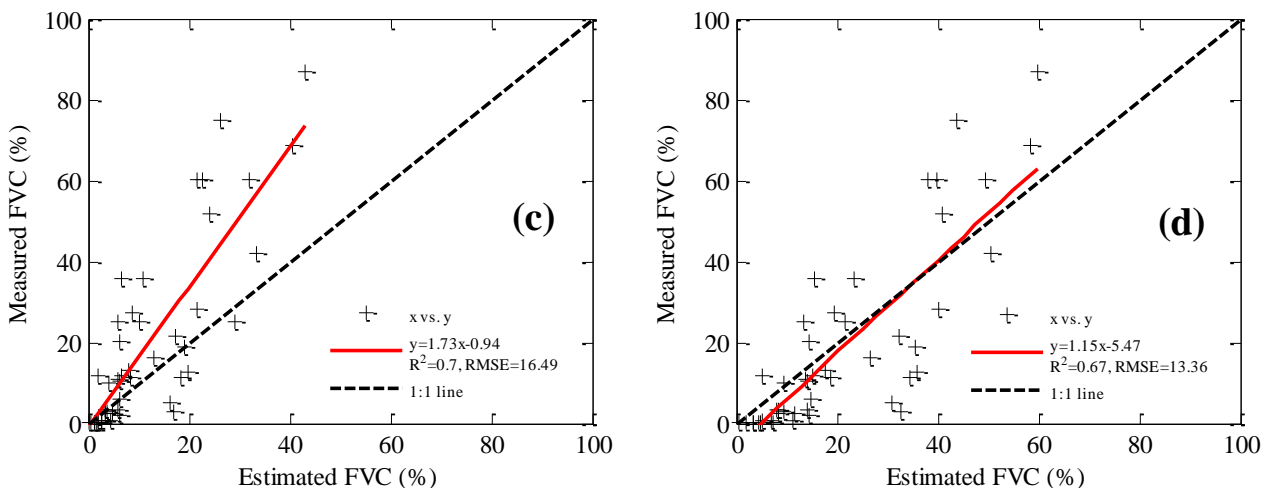
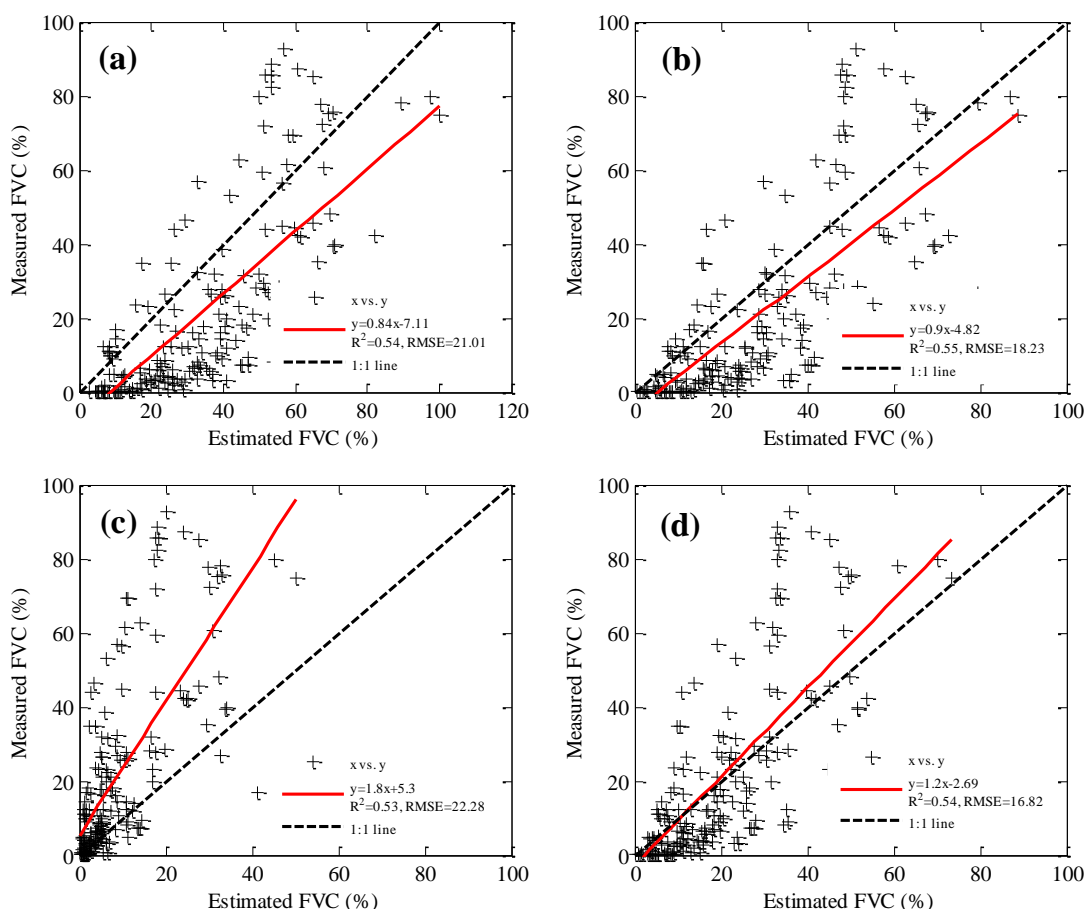


Figure 5. Cont.



**Figure 6.** Accuracy comparisons for estimating grassland FVC for 30 m pixels. (a) uses NDVI as the parameters of Equation (7), where  $NDVI_{soil}$  is 0.119, and  $NDVI_{veg}$  is 0.807 (Table 3); (b) and (c) use NDVI and RVI, respectively, as the parameters of Equation (11), where  $NDVI_{veg}$  is also equal to 0.807, but  $NDVI_{soil}$  and  $RVI_{soil}$  were calculated using remote sensing data from the early growing season (for 13 April, the earliest availability of Landsat 8 data products in 2013 for Inner Mongolia) for soil background measurement; and (d) averages the results from (b) and (c). NDVI and RVI were extracted from Landsat 8 data based on the coordinates of the sample plots.

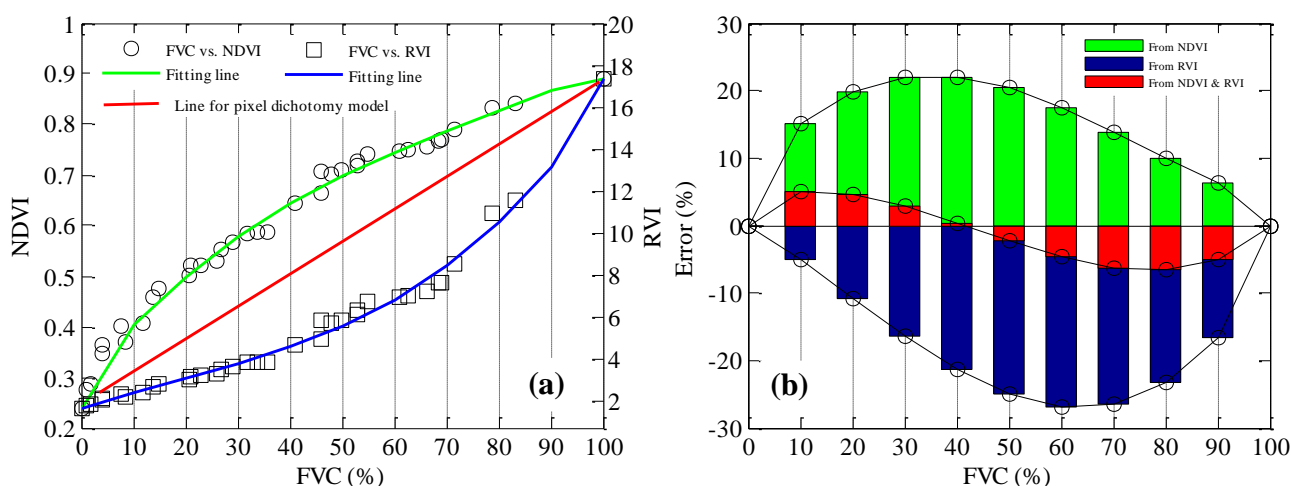


### 4. Discussions

#### 4.1. Sensitivity of NDVI and RVI to FVC

Over the past two decades, NDVI and RVI have been widely used to monitor vegetation biophysical properties such as leaf area index (LAI), FVC, chlorophyll content and biomass [33,45]. However, they have been criticized for problems of sensitivity to the vegetation canopy [36]. For example, NDVI initially increases near-linearly with increasing vegetation density, but the slope of this relationship decreases with higher vegetation density levels, and then enters an asymptotic phase in which NDVI increases very slowly (green line in Figure 7a). This so-called NDVI saturation has been reported by numerous studies [46–50]. Several studies have also found that the relationship between NDVI and FVC is nonlinear [23,50,51]. Consequently, linear SMA, such as the pixel dichotomy model, most likely produces errors in estimating FVC. Figure 7a shows sensitivity changes for NDVI with increasing FVC. It is a convex curve as FVC changes, but the NDVI based pixel dichotomy model (red line in Figure 7a) only matches at the ends of this curve. Therefore, FVC is overestimated when the NDVI based pixel dichotomy model is used. Figure 7b shows that maximum positive errors in excess of 20% from the NDVI-based FVC occur with FVC values between 30% and 40%, and then lessen on either side. RVI has the opposite problem from NDVI for sensitivity (blue line in Figure 7b) since it is equivalent to the exponential transform of NDVI Equation (9). Figure 7a shows that FVC is underestimated using RVI-based FVC except for the two end points (FVC = 0 and 100%). Figure 7b shows that maximum negative errors, again above 20%, from the RVI-based FVC occur with FVC between 60% and 70%, and then lessen on either side. Combining these two indices produces markedly lower errors for FVC estimation (red bars in Figure 7b). Minimum errors occur with FVC around 0%, 40% and 100%, with maximum positive and negative errors occurring with FVC between 10%–20% and 70%–80%, respectively.

**Figure 7.** (a) Sensitivity of NDVI and RVI with increasing FVC; (b) error distribution for FVC estimation using NDVI, RVI and combined NDVI-RVI based SMA models.

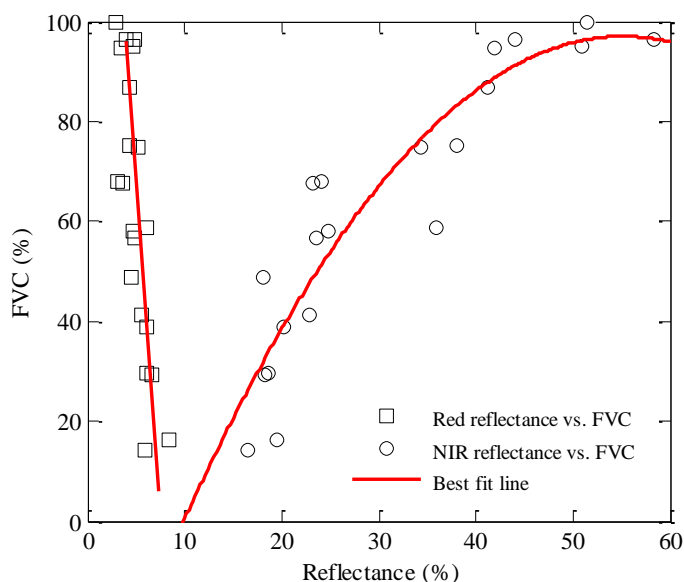


In this study, NDVI and RVI are given equal weights in the combination (each set at 0.5). Figure 7b shows that the lowest estimation errors occur with a FVC of around 40%. If more weight is given to NDVI, and less to RVI, the lowest estimation errors migrate toward higher FVC values; if less weight

is given to NDVI, errors migrate in the opposite direction toward lower FVC values. Equal weighting for NDVI and RVI is simple and effective for canceling out the inherent biases in NDVI and RVI based FVC, although they are not necessarily the optimum weights for minimizing FVC estimation errors.

Jiang *et al.* [50] concluded that the presence of shadow leads to NDVI saturation, which then results in the overestimation of FVC. In fact, NDVI saturation is mainly controlled by near-infrared reflectance from the vegetation canopy, as shown in Figure 8. Compared with red reflectance which ranges only from 0% to 10%, near infrared reflectance ranges from 10 to 60% and determines almost all NDVI change.

**Figure 8.** Sensitivity of red and near-infrared reflectance to FVC.



#### 4.2. Model Comparisons

Jiang *et al.* [50] analyzed the spatial scale dependencies of NDVI and the relationship between NDVI and FVC based on linear SMA models using experimental field data. He argued that NDVI may not be suitable for the retrieval of FVC because of nonlinearity and scale effects. The scaled difference vegetation index (SDVI), which is a scale-invariant index, was then proposed for retrieval of FVC, expressed as:

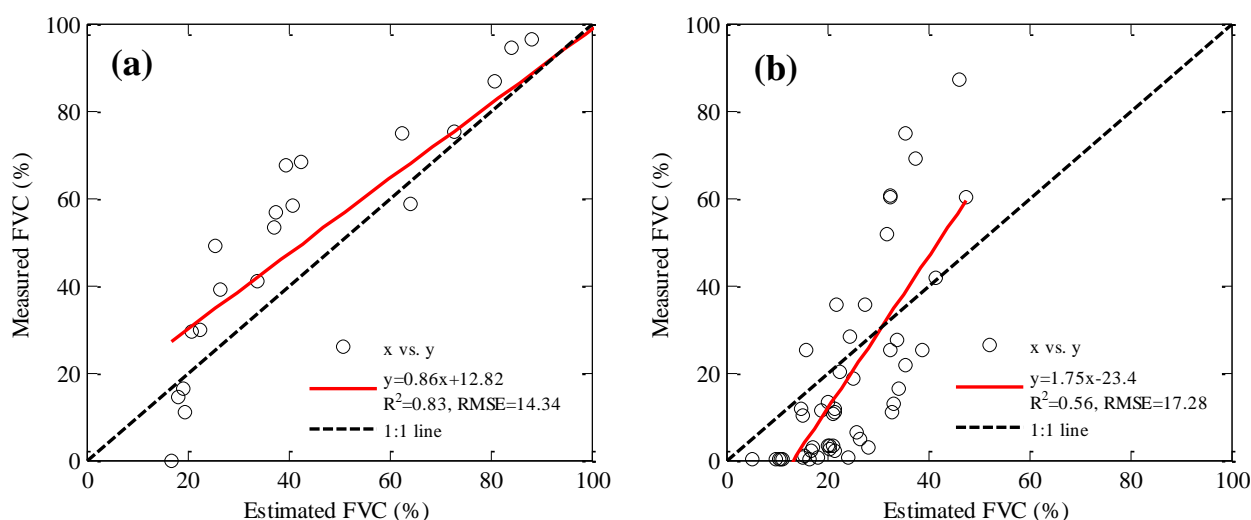
$$f_c = \frac{DVI - DVI_{soil}}{DVI_{veg} - DVI_{soil}} \quad (14)$$

where *DVI* is the difference vegetation index defined as the difference between near-infrared and red reflectance (nir-red); the subscripts, *soil* and *veg*, denote pure endmembers for bare soil and full vegetation cover, respectively.

Figure 9 evaluates SDVI-based FVC estimation at different resolutions including  $0.5 \times 0.5$  m quadrats and  $250 \times 250$  m MODIS pixels. At both resolutions, the estimates are erratic over the entire 0%–100% FVC value scale primarily because DVIs from vegetation canopy spectrums derived from *in situ* measurements and satellite remote sensing are neither stable nor directly comparable. The impacts of atmospheric conditions and differences in the spatial resolution of data collected from

different sensors (evident in Figure 4) are largely responsible. Following [36,50], in Equation (14) the near-infrared and red reflectances for bare soil were set at 0.11 and 0.08, respectively, and for full vegetation cover at 0.5 and 0.05. However, these values generally change with many factors such as soil types, vegetation types and atmospheric conditions, as well as scaling [52]. It becomes very difficult to endorse this approach, especially for satellite remote sensing which is characterized by atmospheric effects and multi-temporal changes. In contrast, VIs with the ratio relationship such as RVI and NDVI can minimize these influences and enhance comparability of VIs derived from different remote sensing data sources and times. It further suggests that the selection of VIs for FVC estimation is crucial. For estimation accuracy, it is important to consider influences from the atmosphere and topography, as well as different remote sensing data sources.

**Figure 9.** Evaluating SDVI-based FVC; (a) at the 0.5 × 0.5 m quadrat scale; and (b) at 250 × 250 m MODIS-pixel scale.



### 4.3. Grassland FVC Changes in Inner Mongolia

Based on Equation (11) and the methods for determining  $NDVI_{soil}$  and  $NDVI_{veg}$  discussed in Section 3.2, MOD09Q1 data for the accrued days of 97 (7 April) and 217 (5 August) from 2000 to 2013 were used to estimate grassland FVC for all of Inner Mongolia. In 2013, Figure 10a shows that most grassland is sparsely distributed. Areas of FVC with less than 20% grassland account for 37.3% of the total area, and areas with less than 50% cover 69.9%. In terms of regional distribution, FVC in middle Inner Mongolia is very sparsely distributed with large areas of FVC less than 10%. Human activity such as overgrazing in these areas is still intense [39,53].

For the period 2000–2013, Equation (15) was used to examine spatial variation in grassland FVC changes in Inner Mongolia, expressed as:

$$FVC_i = a + bT_i \tag{15}$$

where  $T_i$  is a time variable ( $i$  is annual values from 2000 to 2013);  $FVC_i$  is FVC in year  $i$ ; and  $a$  and  $b$  are regression coefficients. This regression trend line was calculated for each pixel and the slopes ( $b$  in Equation (15) are mapped in Figure 10b to explore the spatial variation in grassland FVC change for the 2000–2013 period. Positive values indicate an increase in FVC over time, negative values indicate

a decrease, and values close to zero suggest no change. The corresponding coefficient of determination ( $R^2$ ) is mapped in Figure 10c to provide an indicator of the strength of any trend.

**Figure 10.** (a) 2003 grassland FVC in Inner Mongolia; (b) Directional change in FVC from 2000–2013 quantified by the slope of the regression trend line; and (c) strength of the trend quantified by  $R^2$ .

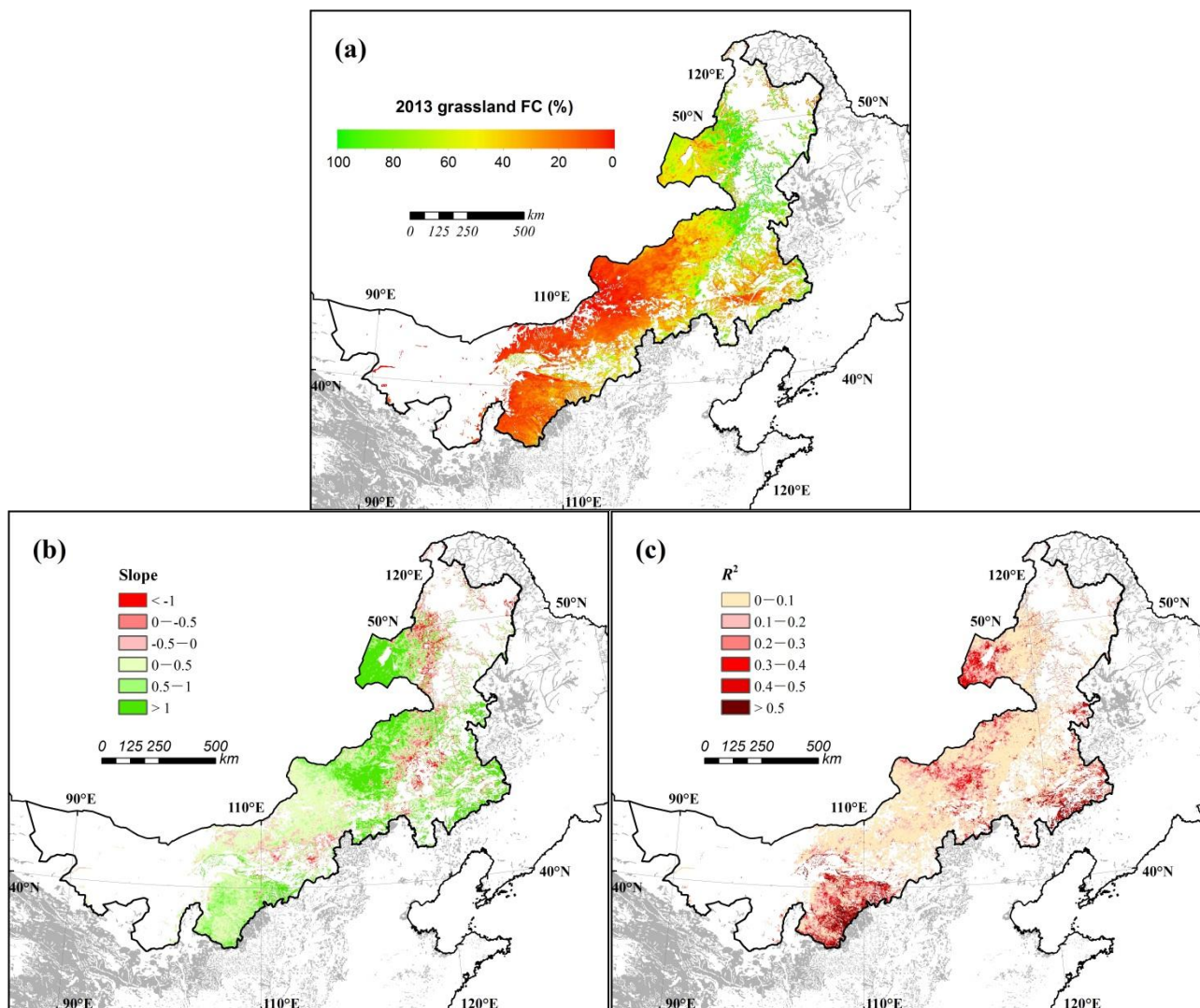


Figure 10b,c show that for most grassland areas there is no strong trend over time, either negative or positive, since the slope is generally close to zero and  $R^2$  is less than 0.1. Exceptions occur in areas of Hulunbeier, south Tongliao, middle Xilin Gol and Erdos, where grassland FVC increases, and in Daxinganling where grassland FVC exhibits a fluctuating decrease.

## 5. Conclusions

The NDVI-based pixel dichotomy model has been commonly used for retrieval of grassland FVC. In practice, FVC was likely overestimated using such models. Substantial positive errors of over 20% occurred with FVC values between 30% and 40%. If RVI is substituted for NDVI, FVC was underestimated, again by over 20%, with the largest errors occurring with FVC values between 60%

and 70%. However, incorporating the average values of both NDVI and RVI effectively cancels out these errors and provides a better result. For grasslands, combining remote sensing data from the early growing season (e.g., accrued day 97 in a year) and *in situ* spectral data measurements can be used to determine the parameters of the pixel dichotomy model including  $VI_{soil}$  and  $VI_{veg}$ . This can simplify the selection of endmembers and improves estimation accuracy.

In this study, the spectral signal gaps for different sensors including portable field spectroradiometers, MODIS and Landsat 8\OLI exist due to the impacts of atmospheric conditions and scale effects. This introduces uncertainties for the endmember value of  $VI_{veg}$ . Further study should focus on reducing these uncertainties. Also, model validation in different regions and with different remote sensing data is needed.

### Acknowledgments

We thank the five anonymous reviewers and Ronald Briggs for their constructive comments and suggestions on the manuscript. This research was funded by the “Strategic Priority Research Program” of the Chinese Academy of Sciences, Climate Change: Carbon Budget and Relevant Issues (Grant No. XDA05050100).

### Conflicts of Interest

The authors declare no conflict of interest.

### Author Contributions

Fei Li was responsible for the data analysis and wrote the majority of the paper. Bingfang Wu supervised the research and contributed to manuscript organization. Wei Chen collected the field data and preprocessed remote sensing data. Yuan Zeng and Qianjun Zhao provided assistances in writing, editing and data analysis.

### References

1. Jiapaer, G.; Chen, X.; Bao, A. A comparison of methods for estimating fractional vegetation cover in arid regions. *Agric. For. Meteorol.* **2011**, *151*, 1698–1710.
2. Adams, J.B.; Sabol, D.E.; Kapos, V.; Almeida, R.; Roberts, D.A.; Smith, M.O.; Gillespie, A.R. Classification of multispectral images based on fractions of endmembers-application to land-cover change in the brazilian amazon. *Remote Sens. Environ.* **1995**, *52*, 137–154.
3. Adams, J.B.; Smith, M.O.; Johnson, P.E. Spectral mixture modeling: A new analysis of rock and soil types at the viking lander 1 site. *J. Geophys. Res.* **1986**, *91*, 8098–8112.
4. Smith, M.O.; Ustin, S.L.; Adams, J.B.; Gillespie, A.R. Vegetation in deserts: I. A regional measure of abundance from multispectral images. *Remote Sens. Environ.* **1990**, *31*, 1–26.
5. Atkinson, P.; Cutler, M.; Lewis, H. Mapping sub-pixel proportional land cover with avhrr imagery. *Int. J. Remote Sens.* **1997**, *18*, 917–935.
6. Pu, R.; Xu, B.; Gong, P. Oakwood crown closure estimation by unmixing landsat tm data. *Int. J. Remote Sens.* **2003**, *24*, 4422–4445.

7. Atzberger, C.; Rembold, F. Mapping the spatial distribution of winter crops at sub-pixel level using AVHRR NDVI time series and neural nets. *Remote Sens.* **2013**, *5*, 1335–1354.
8. Foody, G. Approaches for the production and evaluation of fuzzy land cover classifications from remotely-sensed data. *Int. J. Remote Sens.* **1996**, *17*, 1317–1340.
9. Foody, G.M.; Campbell, N.; Trodd, N.; Wood, T. Derivation and applications of probabilistic measures of class membership from the maximum-likelihood classification. *Photogramm. Eng. Remote Sens.* **1992**, *58*, 1335–1341.
10. DeFries, R.; Hansen, M.; Steininger, M.; Dubayah, R.; Sohlberg, R.; Townshend, J. Subpixel forest cover in central africa from multisensor, multitemporal data. *Remote Sens. Environ.* **1997**, *60*, 228–246.
11. Yang, L.; Huang, C.; Wylie, B.K.; Coan, M.J. An approach for mapping large-area impervious surfaces: Synergistic use of Landsat-7 ETM+ and high spatial resolution imagery. *Can. J. Remote Sens.* **2003**, *29*, 230–240.
12. Tottrup, C.; Rasmussen, M.; Eklundh, L.; Jönsson, P. Mapping fractional forest cover across the highlands of mainland southeast Asia using MODIS data and regression tree modelling. *Int. J. Remote Sens.* **2007**, *28*, 23–46.
13. Elmore, A.J.; Mustard, J.F.; Manning, S.J.; Lobell, D.B. Quantifying vegetation change in semiarid environments: Precision and accuracy of spectral mixture analysis and the Normalized Difference Vegetation Index. *Remote Sens. Environ.* **2000**, *73*, 87–102.
14. Rashed, T.; Weeks, J.R.; Roberts, D.; Rogan, J.; Powell, R. Measuring the physical composition of urban morphology using multiple endmember spectral mixture models. *Photogramm. Eng. Remote Sens.* **2003**, *69*, 1011–1020.
15. Roberts, D.A.; Gardner, M.; Church, R.; Ustin, S.; Scheer, G.; Green, R. Mapping chaparral in the Santa Monica Mountains using multiple endmember spectral mixture models. *Remote Sens. Environ.* **1998**, *65*, 267–279.
16. Small, C. Estimation of urban vegetation abundance by spectral mixture analysis. *Int. J. Remote Sens.* **2001**, *22*, 1305–1334.
17. Small, C. High spatial resolution spectral mixture analysis of urban reflectance. *Remote Sens. Environ.* **2003**, *88*, 170–186.
18. Wu, C.; Murray, A.T. Estimating impervious surface distribution by spectral mixture analysis. *Remote Sens. Environ.* **2003**, *84*, 493–505.
19. Montandon, L.; Small, E. The impact of soil reflectance on the quantification of the green vegetation fraction from NDVI. *Remote Sens. Environ.* **2008**, *112*, 1835–1845.
20. Zhou, X.; Guan, H.; Xie, H.; Wilson, J. Analysis and optimization of NDVI definitions and areal fraction models in remote sensing of vegetation. *Int. J. Remote Sens.* **2009**, *30*, 721–751.
21. Asner, G.P.; Heidebrecht, K.B. Spectral unmixing of vegetation, soil and dry carbon cover in arid regions: Comparing multispectral and hyperspectral observations. *Int. J. Remote Sens.* **2002**, *23*, 3939–3958.
22. Borel, C.C.; Gerstl, S.A. Nonlinear spectral mixing models for vegetative and soil surfaces. *Remote Sens. Environ.* **1994**, *47*, 403–416.
23. Huete, A.; Jackson, R.; Post, D. Spectral response of a plant canopy with different soil backgrounds. *Remote Sens. Environ.* **1985**, *17*, 37–53.

24. Huete, A.R. Separation of soil-plant spectral mixtures by factor analysis. *Remote Sens. Environ.* **1986**, *19*, 237–251.
25. Gutman, G.; Ignatov, A. The derivation of the green vegetation fraction from NOAA/AVHRR data for use in numerical weather prediction models. *Int. J. Remote Sens.* **1998**, *19*, 1533–1543.
26. Qi, J.; Marsett, R.; Moran, M.; Goodrich, D.; Heilman, P.; Kerr, Y.; Dedieu, G.; Chehbouni, A.; Zhang, X. Spatial and temporal dynamics of vegetation in the San Pedro River basin area. *Agric. For. Meteorol.* **2000**, *105*, 55–68.
27. Wittich, K.; Hansing, O. Area-averaged vegetative cover fraction estimated from satellite data. *Int. J. Biometeorol.* **1995**, *38*, 209–215.
28. Zeng, X.; Dickinson, R.E.; Walker, A.; Shaikh, M.; DeFries, R.S.; Qi, J. Derivation and evaluation of global 1-km fractional vegetation cover data for land modeling. *J. Appl. Meteorol.* **2000**, *39*, 826–839.
29. Theseira, M.; Thomas, G.; Sannier, C. An evaluation of spectral mixture modelling applied to a semi-arid environment. *Int. J. Remote Sens.* **2002**, *23*, 687–700.
30. Xiao, J.; Moody, A. A comparison of methods for estimating fractional green vegetation cover within a desert-to-upland transition zone in central New Mexico, USA. *Remote Sens. Environ.* **2005**, *98*, 237–250.
31. Peterson, S.; Stow, D. Using multiple image endmember spectral mixture analysis to study chaparral regrowth in southern California. *Int. J. Remote Sens.* **2003**, *24*, 4481–4504.
32. Shoshany, M.; Svoray, T. Multidate adaptive unmixing and its application to analysis of ecosystem transitions along a climatic gradient. *Remote Sens. Environ.* **2002**, *82*, 5–20.
33. Leprieur, C.; Kerr, Y.; Mastorchio, S.; Meunier, J. Monitoring vegetation cover across semi-arid regions: Comparison of remote observations from various scales. *Int. J. Remote Sens.* **2000**, *21*, 281–300.
34. Messina, J.; Delamater, P. Defoliation and the war on drugs in Putumayo, Colombia. *Int. J. Remote Sens.* **2006**, *27*, 121–128.
35. Zhang, X.; Liao, C.; Li, J.; Sun, Q. Fractional vegetation cover estimation in arid and semi-arid environments using HJ-1 satellite hyperspectral data. *Int. J. Appl. Earth Observ. Geoinf.* **2012**, *21*, 506–512.
36. Carlson, T.N.; Ripley, D.A. On the relation between NDVI, fractional vegetation cover, and leaf area index. *Remote Sens. Environ.* **1997**, *62*, 241–252.
37. Delamater, P.L.; Messina, J.P.; Qi, J.; Cochrane, M.A. A hybrid visual estimation method for the collection of ground truth fractional coverage data in a humid tropical environment. *Int. J. Appl. Earth Observ. Geoinf.* **2012**, *18*, 504–514.
38. Kawamura, K.; Akiyama, T.; Yokota, H.-O.; Tsutsumi, M.; Yasuda, T.; Watanabe, O.; Wang, S. Quantifying grazing intensities using geographic information systems and satellite remote sensing in the Xilingol steppe region, Inner Mongolia, China. *Agric. Ecosyst. Environ.* **2005**, *107*, 83–93.
39. Li, S.G.; Harazono, Y.; Oikawa, T.; Zhao, H.L.; He, Y.Z.; Chang, X.L. Grassland desertification by grazing and the resulting micrometeorological changes in Inner Mongolia. *Agric. For. Meteorol.* **2000**, *102*, 125–137.
40. Sun, X.F.; Yue, T.X.; Wang, Q. High accuracy surface modeling of grassland aboveground biomass. *J. Remote Sens.* **2013**, *17*, 1060–1076.

41. Purevdorj, T.; Tateishi, R.; Ishiyama, T.; Honda, Y. Relationships between percent vegetation cover and vegetation indices. *Int. J. Remote Sens.* **1998**, *19*, 3519–3535.
42. LAADS. Available online: <http://ladsweb.nascom.nasa.gov/> (accessed on 16 May 2014).
43. Irons, J.R.; Dwyer, J.L.; Barsi, J.A. The next Landsat satellite: The Landsat data continuity mission. *Remote Sens. Environ.* **2012**, *122*, 11–21.
44. USGS. Available online: <http://landsat.usgs.gov/> (accessed on 16 May 2014).
45. Huete, A.R.; Liu, H.Q. An error and sensitivity analysis of the atmospheric-and soil-correcting variants of the NDVI for the MODIS-EOS. *IEEE Trans. Geosci. Remote Sens.* **1994**, *32*, 897–905.
46. Baret, F.; Guyot, G. Potentials and limits of vegetation indices for LAI and APAR assessment. *Remote Sens. Environ.* **1991**, *35*, 161–173.
47. Gitelson, A.A. Wide dynamic range vegetation index for remote quantification of biophysical characteristics of vegetation. *J. Plant Physiol.* **2004**, *161*, 165–173.
48. Haboudane, D.; Miller, J.R.; Pattey, E.; Zarco-Tejada, P.J.; Strachan, I.B. Hyperspectral vegetation indices and novel algorithms for predicting green LAI of crop canopies: Modeling and validation in the context of precision agriculture. *Remote Sens. Environ.* **2004**, *90*, 337–352.
49. Vescovo, L.; Gianelle, D. Using the MIR bands in vegetation indices for the estimation of grassland biophysical parameters from satellite remote sensing in the Alps region of Trentino (Italy). *Adv. Space Res.* **2008**, *41*, 1764–1772.
50. Jiang, Z.; Huete, A.R.; Chen, J.; Chen, Y.; Li, J.; Yan, G.; Zhang, X. Analysis of NDVI and scaled difference vegetation index retrievals of vegetation fraction. *Remote Sens. Environ.* **2006**, *101*, 366–378.
51. Colwell, J.E. Vegetation canopy reflectance. *Remote Sens. Environ.* **1974**, *3*, 175–183.
52. Obata, K.; Wada, T.; Miura, T.; Yoshioka, H. Scaling effect of area-averaged NDVI: Monotonicity along the spatial resolution. *Remote Sens.* **2012**, *4*, 160–179.
53. Zou, C.; Wang, K.; Wang, T.; Xu, W. Overgrazing and soil carbon dynamics in eastern Inner Mongolia of China. *Ecol. Res.* **2007**, *22*, 135–142.